
# Effect of phase separation and supercooling on the storage capacity in a commercial latent heat thermal energy storage: Experimental cycling of a

Downloaded from: https://research.chalmers.se, 2026-04-04 13:27 UTC

Citation for the original published paper (version of record):
Tan, P., Lindberg, P., Eichler, K. et al (2020). Effect of phase separation and supercooling on the storage capacity in a commercial latent heat
thermal energy storage: Experimental cycling of a salt hydrate PCM. Journal of Energy Storage, 29.
http://dx.doi.org/10.1016/j.est.2020.101266

N.B. When citing this work, cite the original published paper.

research.chalmers.se offers the possibility of retrieving research publications produced at Chalmers University of Technology. It covers all kind of research output: articles, dissertations, conference papers, reports etc. since 2004. research.chalmers.se is administrated and maintained by Chalmers Library

(article starts on next page)

# Effect of Phase Separation and Supercooling on the Storage Capacity in a Commercial Latent Heat Thermal Energy Storage: Experimental Cycling of a Salt Hydrate PCM

Pepe Tan[a,*], Patrik Lindberg[b], Kaia Eichler[b], Per Löveryd[c], Pär Johansson[a], Angela Sasic Kalagasidis[a]

[a] *Department of Architecture and Civil Engineering, Division of Building Technology, Chalmers University of Technology, Gothenburg, Sweden*
[b] *ÅF Pöyry AB, Gothenburg, Sweden*
[c] *Akademiska Hus AB, Gothenburg, Sweden*

**Abstract**

Latent heat storage technologies offer process benefits like daily peak shaving. In this work a commercial storage design for storing cold thermal energy has been studied using a laboratory prototype containing 168 kg of a commercial salt-hydrate phase change material (PCM). The storage was charged and discharged with subsequent cycles at different mass flow rates over a fixed temperature range and duration. It was found that the PCM TES design exhibits phase separation and increased supercooling with continuous cycling. Both phenomena lead to a gradual decrease of the effective storage capacity. With later cycles only the bottom part stores latent heat, while the top and middle parts of the storage remain liquid. The results were repeatable and are consistent with T-History measurements of samples from

*Corresponding author
*Email address:* pepe.tan@chalmers.se (Pepe Tan)

the PCM TES before and after cycling. It is likely that the PCM itself does not suffer from incongruent melting. Instead, the phase separation is likely to occur due to a segregation of different liquid phases across the height of the storage. It was found that T-History measurements alone are not able to predict this behavior. Moreover, it is shown that phase separation in the storage can be reversed by increasing the PCM temperature and mechanical mixing of the liquid phase. This phase separation has to be prevented in future work in order to achieve stable performance with the studied storage design.
*Keywords:* Thermal Energy Storage, Phase Change Materials, Phase Separation, Supercooling, Salt-Hydrate

## 1. Introduction

Integrating a thermal energy storage (TES) in the energy supply system of buildings allows the operator a greater range of process flexibility and the possibility to utilize intermittent energy [1]. It is therefore seen as a key technology in order to facilitate the transition from fossil fuels to renewable energy sources.

In recent years, the interest in using the latent heat of melting and solidification of so called phase change materials (PCMs) has gained considerable attention among researchers [2, 3]. This is due to their ability to store significant amounts of latent heat, which allows for higher storage densities compared to sensible storage technologies and consequently less space is required for energy storage solutions. Their use is therefore particularly interesting for applications with a small temperature range available for charging and

discharging the storage. A PCM TES, typically consists of a heat exchanger in which a heat transfer fluid (HTF) is used to melt and solidify the PCM. Various heat exchanger concepts have been studied in the literature with different PCMs.

Despite the research interest, actual real scale applications are few due to high costs and well-known design challenges depending on the chosen material [4]. In particular salt-hydrates are considered to be a promising material and therefore widely available as a commercial product [5, 6]. Salt-Hydrates offer the following benefits:

- Relatively low cost (e.g. compared to paraffins based on fossil fuels)
- High storage density
- Higher thermal conductivity (e.g. compared to paraffins)

However, they are also known for severe problems that have to be taken into account in the heat exchanger design:

- Corrosive to metals
- Supercooling
- Phase separation / Incongruent melting

An important research objective is therefore to evaluate how a Salt-Hydrate PCM performs in a heat exchanger design when it is operated within application boundaries such as a predefined temperature range for the HTF to solidify and melt the PCM.

Corrosion of salt-hydrates in combination with different materials have been studied in the literature before [7, 8]. For the relatively low temperatures of building applications, corrosion can be prevented when a suitable heat exchanger material is used, such as plastics. The downside is that low heat transfer rates are expected due to low thermal conductivities compared to metals.

Supercooling occurs when the liquid PCM cools down below its theoretical solidification/melting temperature before solidification starts. It is a major risk in the storage design because when the liquid PCM is able to cool down to lower temperatures than the charging temperature in cold storage applications, the PCM will not solidify and latent heat can not be stored. Studies on supercooling have been done mostly on material scale with continuous cycling in differential scanning calorimeters (DSC) [9]. Among the few works studying supercooling on laboratory storages, Rathgeber et al. [10] showed that significantly different results in regards to supercooling can be observed depending on the experimental scale. In their study, the degree of supercooling of the studied PCMs decreased from DSC samples to a storage prototype. This is because supercooling is seen as a stochastic process. The probability for supercooling decreases with larger scale, especially when a PCM solid phase or nucleating agents are already present in the storage, from which nucleation can occur. It is generally recommended to use different complementary scales in order to rule out the influence of the sample size on the supercooling behavior [11].

The terms phase separation and incongruent melting are typically used interchangeably and have been studied on material scale early on [12, 13, 3].

Incongruent melting is defined as when a new solid and liquid phase of different compositions may precipitate from the original composition with each melting and solidification cycle. In severe cases, the new compositions may have a different melting and solidification range compared to the original mixture. When these temperatures are outside of the application temperature range for charging and discharging, the material will not participate in the next melting and solidification cycles. A degradation of the storage capacity is therefore observed unless the temperature range is adjusted and the initial composition is restored. Typically, this can be done by bringing the material to a complete liquid state and mixing the liquid phase. This effect can be prevented if the initial composition of the PCM is adjusted to circumvent the region of incongruent melting [14, 15]. Phase diagrams are in this case very useful [16]. Incongruent melting is observable already on material scale, since it is an intrinsic problem due to a unstable material composition. Previous works have typically also utilized DSC measurements to study the effect of phase separation [14].

Both supercooling and phase separation are phenomena that cause the observed storage capacity to degrade if the PCM is not able to solidify or melt within the given process temperature range for charging and discharging. It is notable that while salt-hydrates have been studied commonly on material scale, lab scale studies using storage prototypes or real scale PCM TES are rare.

Zondag et al. [17] observed that a salt-hydrate storage prototype based on $MgCl_2 \cdot 6H_2O$ as PCM yielded a lower storage capacity than it was measured with DSC samples due to phase separation. Alam et al. [18] reported that a

discrepancy of manufacturer values of a commercial salt-hydrate resulted in poor performance of a full scale PCM TES during actual operation within the building energy system. The material exhibited more severe supercooling as well as a lower storage capacity compared to the manufacturer specification. As an end result only as low as 15 % of the installed storage capacity was usable. A similar observation was done by Jokiel [19] for the same storage design and supplier in an installation in Norway.

It is therefore highly relevant to study storage designs in a laboratory prototype and under the same operational conditions as of the intended application to derive conclusions regarding the suitability of a storage design. Moreover, these results should be used to verify whether measurements on material scale are representative for the application. This is especially important when commercial salt-hydrates are used, for which the exact composition is not known.

### *1.1. Research Objectives*

The aim of this study is to experimentally evaluate a latent heat storage design with a commercially available salt-hydrate as PCM in terms of power output and storage capacity during charging and discharging.

In this work, a laboratory scale PCM storage was built and a test setup was constructed around the storage. The laboratory storage is a smaller version of a full size storage design, which was offered as a commercial solution for a large scale PCM cold storage project in a new office building on the Chalmers University of Technology Campus Johanneberg in Gothenburg, Sweden [20, 21].

The intended application of the storage is to contribute to daily peak

shaving by storing cold energy within a temperature difference of about 10 °C. It is intended to store cold energy during the night at low energy prices and providing cold energy to the building during the day to avoid peaks in energy prices. The storage is located in an office building connected to a district cooling network. It is charged from a district cooling substation with water at 7-8 °C. Discharging occurs with a water temperature of 16-18 °C at the storage inlet coming from the return line of the air handling unit (AHU) of the building. The latter provides comfort cooling by distributing cold air with variable volume flow. During discharging, the storage is designed to cool down the return line to a maximum temperature of about 14 °C.

The laboratory scale storage is tested with the same application parameters in order to study the performance of the PCM within the storage with regards to the previously mentioned risks. To the best of the author's knowledge this storage design in combination with the commercial salt-hydrate has not been previously reported in the literature.

## 2. Material and Methods

The following sections describe firstly the laboratory storage in detail. Then the test setup and the experimental parameters are presented. Lastly, the analysis method is presented, with which the experimental results are evaluated.

### *2.1. PCM TES Description*

Fig. 1a shows the PCM TES. The storage container consists of a acrylic glass (plexiglass, PMMA) tank. It has interior dimensions of 560x560x800 mm (LxWxH) and a 30 mm wall thickness of the acrylic glass. The acrylic

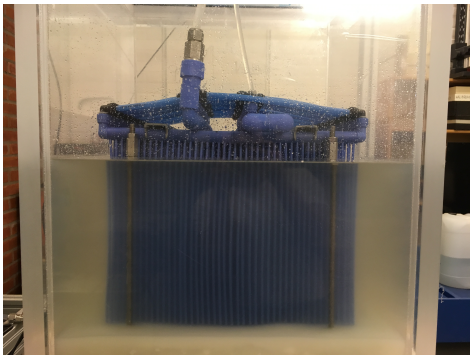

(a) Photo of PCM TES showing the heat exchanger and surrounding SP11

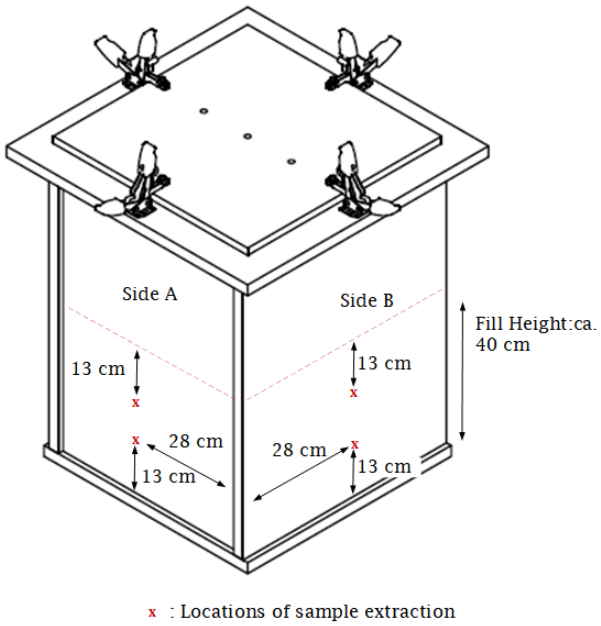


(b) Sketch of the acrylic glass container

Figure 1: PCM TES

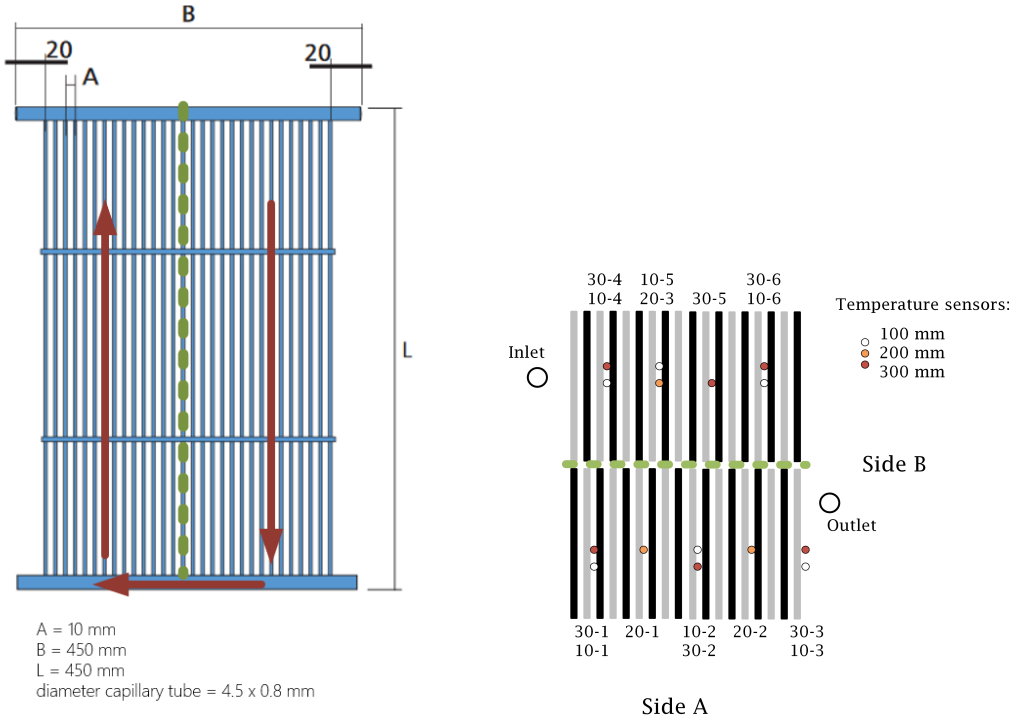


(a) Capillary tube mat geometry (b) Temperature sensor positions

Figure 2: Capillary tube mat and temperature sensors. The grey and black colors in (b) indicate alternating flow directions for each capillary mat.

glass tank is custom made by a local workshop and the design is based on vacuum chamber designs, where clamps are pressing a removable lid and sealing on the tank body for air tightness (Fig. 1b).

The tank is filled with 168 kg of the commercially available salt-hydrate SP11 [22] with a manufacturer stated phase transition temperature of about 11 °C and storage capacity of 4.92 kW h (Tab. 1). According to the material safety data sheet, its main salt components are ammonium chloride, sodium acetate and sodium formate. The exact concentration of each component or

any additives is unknown to the authors. According to Tab. 1 the maximum possible storage density is about three times larger than a water storage of the same volume $\delta_{max}^{Water} \approx 11.6\,\mathrm{kW\,h\,m^{-3}}$ within the application temperature difference of $\Delta T = 10\,\mathrm{K}$.

The heat exchanger is placed inside the PCM liquid and consists of 18 capillary tube mats made from polypropylene random copolymer (see Fig. 2a). The heat exchanger concept is also commercially available as SP.ICE using Water/Ice as PCM [23]. The tube to tube distance is with 10 mm narrow, since only a thin PCM layer around the heat exchanger can be efficiently utilized as storage material. It was shown by the authors previously that a wider PCM layer may not necessarily lead to higher storage densities [21]. This is because of the low thermal conductivity of the PCM preventing an efficient injection and extraction of latent heat.

Each mat has one collector pipe on top and bottom, which distributes the HTF to the smaller capillary tubes (44 in each mat). In a mat, the top collector pipe is separated midway so that the flow follows a U-shape through 22 of the capillary tubes. Half of the total number of capillaries are thus connected parallel to the supply and return pipes and the effective length for heat exchange is twice the length of a single capillary. All mats are in turn connected to a single supply and return pipe for the whole heat exchanger.

Compared to the laboratory storage, the full scale storage's interior dimensions designed to be 2.6x1.8x1.68 m (LxWxH), containing 100 mats and 172 capillary tubes per mat.

Six PT100 temperature sensors are placed between the mats at 10 cm

and 30 cm depths each and an additional three are placed at 20 cm depth to record temperature changes of the PCM (Fig. 2b). The PCM TES is insulated on the exterior side with 65 mm removable extruded polystyrene foam (XPS) boards.

Table 1: PCM TES specifications

| Property | Value | Comment |
|---|---|---|
| $m_{PCM}$ | 168 kg | |
| $V_{PCM}$ | 125.37 L | |
| $\rho_{PCM}$ | 1340 kg m$^{-3}$ | Manufacturer value at 20 °C |
| $T_{PCM}$ | 11 K | Manufacturer value |
| $\Delta h_{max}$ | 0.0293 kW h kg$^{-1}$ | Manufacturer estimate for the application temperature difference of ca. 10 °C |
| $N_{mats}$ | 18 | |
| $d_{mats}$ | 25 mm | center-center distance between mats |
| $d_{tubes}$ | 10 mm | center-center distance between tubes in each mat |
| $N_{tubes}$ | 792 | 396 parallel connected |
| $V_{HEX}$ | 10.5 L | External volume of mats in contact with PCM |
| $V_{TES}$ | 135.87 L | $V_{PCM} + V_{HEX}$ |
| $Q_{max}$ | 4.92 kW h | Manufacturer estimate for the application temperature difference of ca. 10 °C |
| $\delta_{max}$ | 36.21 kW h m$^{-3}$ | $\frac{Q_{max}}{V_{TES}}$ |

*2.2. Experimental Setup*

Fig. 3 shows the experimental test setup used in this work. It consists of a primary loop in which water as HTF is circulated through the PCM TES. This loop is connected via a plate heat exchanger to a secondary loop. In the secondary loop a Julabo FP51-SL thermostatic bath circulator acts as heat source and sink for the PCM TES. In the primary loop, the TES inlet temperature is controlled via the bath and a constant external temperature set point.

The mass flow rate is set before each experiment using a manual metering valve and different pump speed settings of the flexible impeller pump. A Rheonik RHM03 coriolis flow meter is used for flow rate measurements.

*2.3. Analysis Method*

The power (W) and capacity (kWh) are calculated based on the mass flow rate and difference of inlet and outlet temperature at each time step.

$$P(t) = \dot{m}_{HTF}(t) \cdot c_p \cdot (T_{in}(t) - T_{out}(t)) \tag{1}$$

$$Q(t) = \int_0^t \left| P(t') \right| dt' \tag{2}$$

For discharging cases, the TES outlet temperature will change depending on the TES state of charge and eventually be equal to $T_{in}$. In real applications there are temperature requirements on $T_{out}(t)$ from the downstream process, for which the TES provides cold energy during discharging. In this work, a cutoff condition on $T_{out}(t = t^*) = 14\,^{\circ}\mathrm{C}$ is used to evaluate the utilizeable storage capacity during discharging ($Q_{eff} = \int_0^{t^*} \left| P(t) \right| dt$). This limit

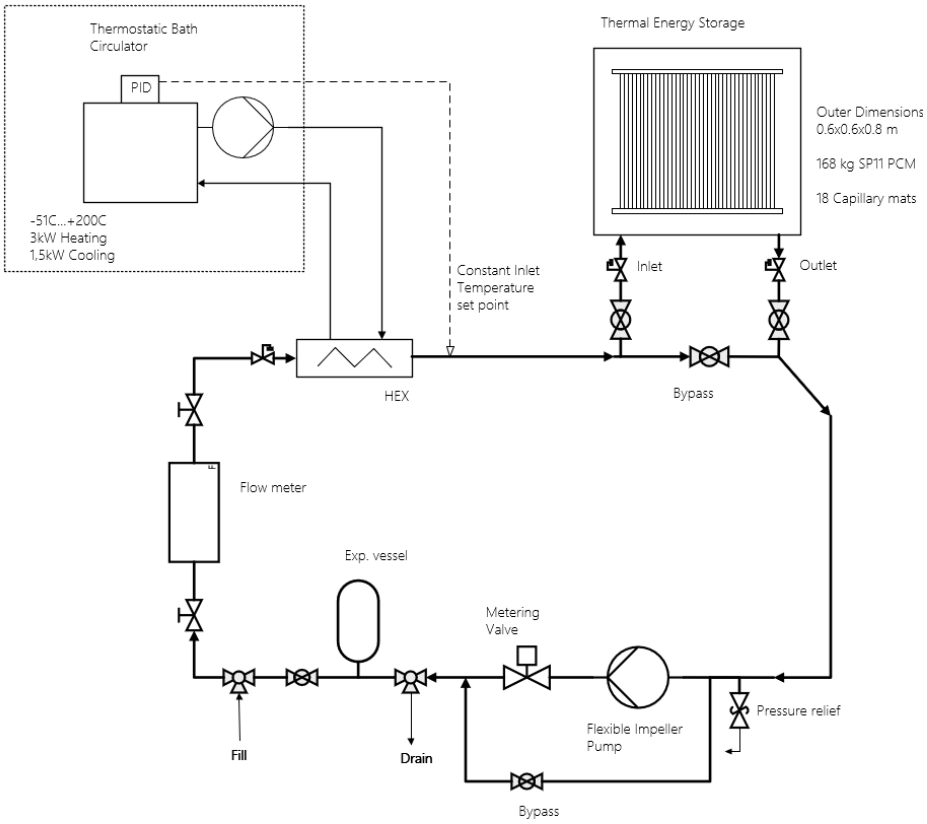


(a) Scheme

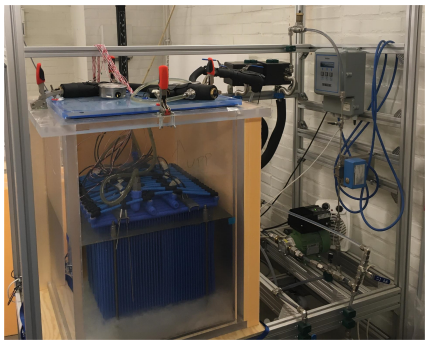

(b) Photo

Figure 3: Experimental Setup of the laboratory scale PCM storage.

is imposed since at higher outlet temperatures, the power for operating the auxiliary equipment (such as pumps) will exceed the power output of the storage at full scale conditions.

A capacity effectiveness (-) can then be defined as a ratio of $Q_{eff}$ and the stated theoretical maximum storage capacity from the manufacturer [21].

$$\eta_Q = \frac{Q_{eff}}{Q_{max}} \tag{3}$$

An effective storage density ($\mathrm{kW\,h\,m^{-3}}$) is given then by:

$$\delta_{eff} = \eta_Q \cdot \delta_{max} \tag{4}$$

The experimental parameters are chosen according to the intended application described above. Since the storage is to be operated as a daily storage, the PCM TES was charged and discharged in 12 hour cycles. In the considered application, the TES can only be charged and discharged using constant inlet temperatures in the range of 7-8 to 16-18 °C, respectively. Therefore, only mass flow rates for charging and discharging are controllable parameters for the storage operator. For the latter, the ranges are given in Tab. 2. These were chosen low enough so that a reasonable percentage of the storage capacity is discharged before the cutoff condition. This is a limitation of heat transfer between the heat transfer fluid and PCM imposed by the heat exchanger design and material properties.

Data collection for mass flow rate and temperatures was done every 10 s using a Keysight 34972A data logger.

In total, six series of experiments with a high, medium and low mass flow rate ranges (HF, MF, LF) are performed over the course of 15 weeks, which

are shown in Tab. 2.

Table 2: Overview of Experiments

| Experiment | $\dot{m}$ ($\mathrm{kg\,min^{-1}}$) | $T_{bath}$ (°C) | No. of cycles (melting/solidification) |
|---|---|---|---|
| HF 1 | $1.375 \pm 0.13$ | $7 - 17$ | (5/4) |
| HF 2 | $1.375 \pm 0.13$ | $7 - 17$ | (8/7) |
| HF 3 | $1.375 \pm 0.13$ | $7 - 17$ | (17/16) |
| MF | $1.0 \pm 0.15$ | $7 - 17$ | (17/16) |
| LF 1 | $0.8 \pm 0.1$ | $5 - 16$ | (4/3) |
| LF 2 | $0.65 \pm 0.05$ | $7 - 17$ | (10/9) |

The Coriolis flow meter is calibrated from the supplier to a expanded (k=2) relative standard uncertainty of ±0.24 % for the experimental range in this work. The temperature sensor calibration expanded uncertainty is estimated to be 0.2 °C. Expanded uncertainty for power is estimated to not exceed 40 W. This was estimated using the largest known uncertainties for flowrate and temperature. The expanded uncertainty for the capacity calculated from Eq. 2 is evaluated using the adaptive Monte Carlo method [24, 25] and is estimated not to exceed 0.02 kWh for all reported experiments.

## 3. Results & Discussion

In the following chapters the experimental results are presented and discussed. First a comparison is done regarding repeatability of the experiments after each cycling. Then the power and capacity measurements are presented together with an interpretation of the results. In the last section, results of T-History measurements are presented that were performed on samples from the tank. These were taken before and after cycling in order to study the phase change temperature and storage capacity of the PCM in more detail.

### *3.1. Repeatability*

After the first cycling experiments a loss of approximately 40 % capacity was observed. Since it was strongly suspected that the PCM suffers from phase separation, the following procedure was performed after each experimental series: (1) The PCM TES was heated up to 45 degC using the HTF to ensure complete melting of the PCM. (2) It was then cooled down to 30 degC and (3) the liquid PCM was manually mixed inside the tank. (4) The storage was then cooled down to 1 degC and approximately 40 mL of solid SP11 (stored at −20 °C) was added to the storage to ensure solidification of any supercooled PCM around the heat exchanger. This amount of solid PCM acts as nucleation point for the supercooled liquid phase. (5) The PCM TES was then allowed to rise to about 7 °C by adjusting the constant HTF inlet temperature via the thermostatic bath for 12 h until all sensors showed approximately the same temperature. The first melting/discharging occasion was performed from this state. This way, it was ensured that the tank was reset and all experiments start approximately from the same state.

Fig. 4 shows that this procedure yielded an acceptable repeatability for the three HF experiments. The first melting occasion is in the following denoted as "Cycle 0" to emphasize that the first cycle depends on this initial state. The first solidification occasion after the initial melting is denoted as "Cycle 1". In the following Cycle 0, Cycle 1 and Cycle 9 are used to compare the different experiments.

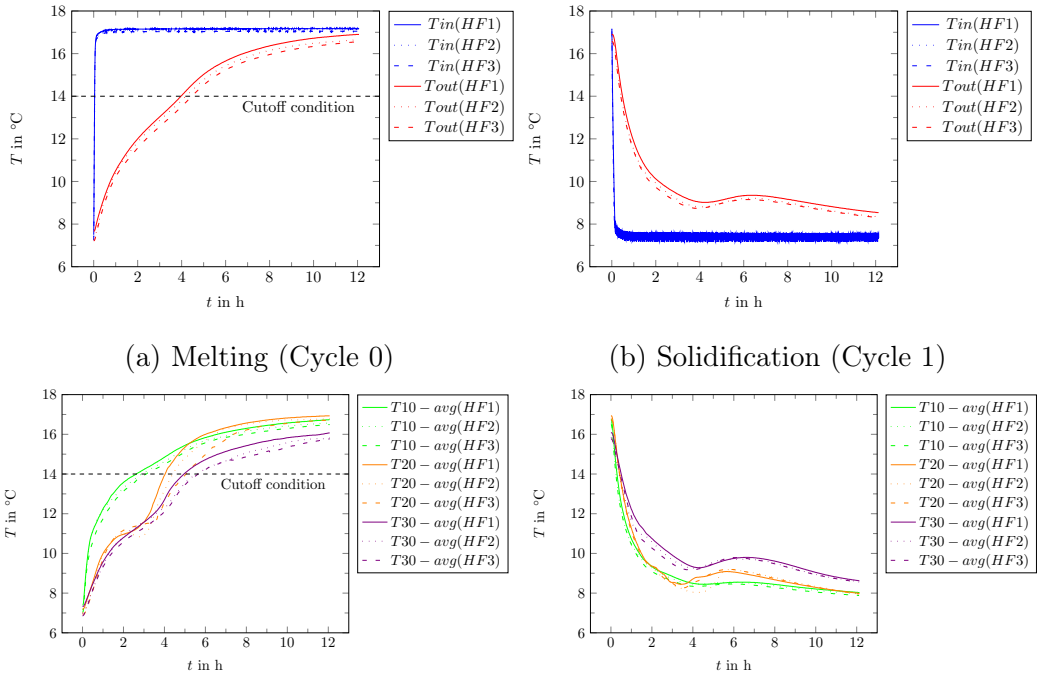


(a) Melting (Cycle 0)

(b) Solidification (Cycle 1)

(c) Melting (Cycle 0)

(d) Solidification (Cycle 1)

Figure 4: Repeatability of HF experiments for the first melting (Cycle 0) and solidification occasion (Cycle 1). T10-,T20- and T30-avg refer to the average of all 10, 20 and 30 cm temperature sensors in the PCM TES, respectively.

*3.2. Power of charging and discharging*

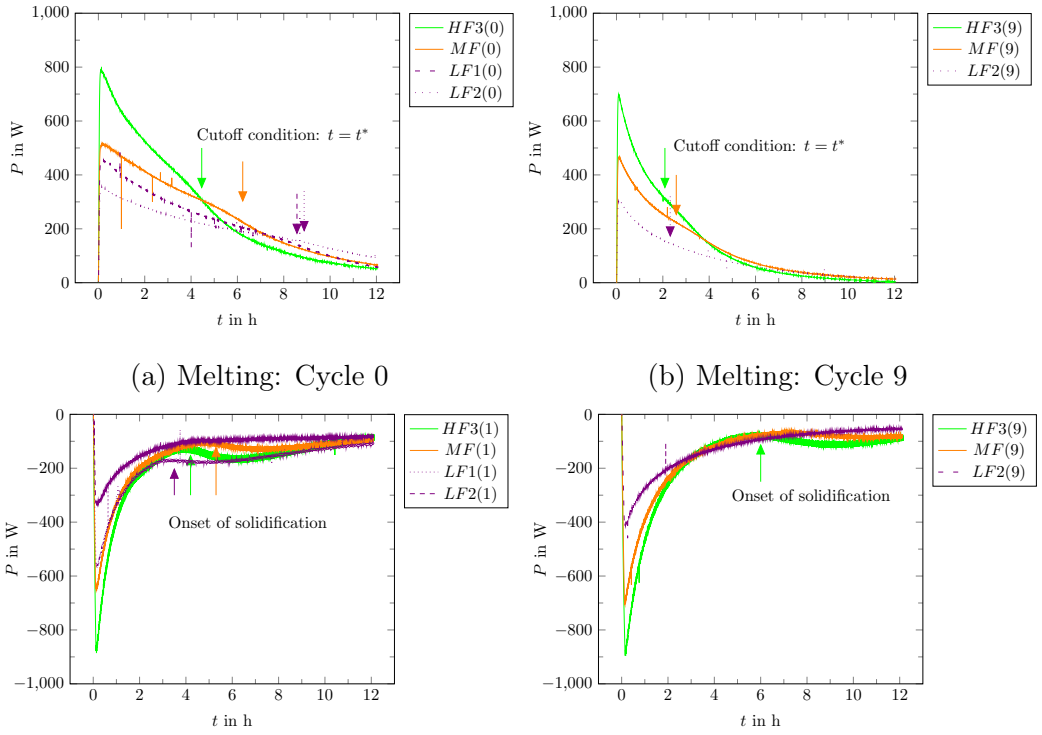


(a) Melting: Cycle 0

(b) Melting: Cycle 9

(c) Solidification: Cycle 1

(d) Solidification: Cycle 9

Figure 5: Charging and discharging power for HF 3, MF and LF 2 for melting (Cycle 0 and 9) and solidification (Cycle 1 and 9)

The discharging and charging power of the PCM TES are reported in Fig. 5 for the different mass flow rate ranges. For the first discharging measurement of Cycle 0 (Fig. 5a), it can be seen that the power output decreases nonlinearly due to the decreasing temperature difference between the in- and outlet temperature of the PCM TES. The average power output is 500 W to 200 W until the cutoff condition from the highest to the lowest mass flow rate cases respectively. For charging in Cycle 1 (Fig. 5c), the power

is decreased due to smaller temperature difference between the solidification temperature of the PCM and the tank inlet temperature. When supercooling occurs, this temperature difference is decreased further. It can be seen that the charging power output rises visibly, due to the PCM solidifying from a supercooled state after 4 to 6 hours in the cases HF 3 and MF. From the graph it can be seen that latent heat is stored in the range of 200 to 100 W only.

However in Fig. 5b and 5d, a decrease in power output is visible with continuous cycling indicating a decrease of the storage capacity after nine cycles. In Fig. 5d only HF 3 shows a visible onset of solidification. It occurs moreover 2 hours delayed compared to solidification Cycle 1. The deviations between the cycles are discussed further in the next sections.

In Fig. 5, outliers are also shown, which are likely due to vibrational noise or single air bubbles affecting the Coriolis flow meter. The noisy data improved with time due to automatic venting valves located at the top part of the experimental setup. Since the data recording rate is high and the noise occurred for a single measurement point, the error for calculating the capacity over a 12 hour duration is negligible.

### *3.3. Loss of capacity*

Fig. 6 show photographs of the tank before and after cycling. Over the course of nine to sixteen charging and discharging cycles the last solidification melting stages have changed visibly compared to the initial state. Fig. 6b and 6c are especially notable, since no difference between the charged and discharged state is visible from the photos alone.

Fig. 7 shows a summary of the measured discharge (melting) and charging

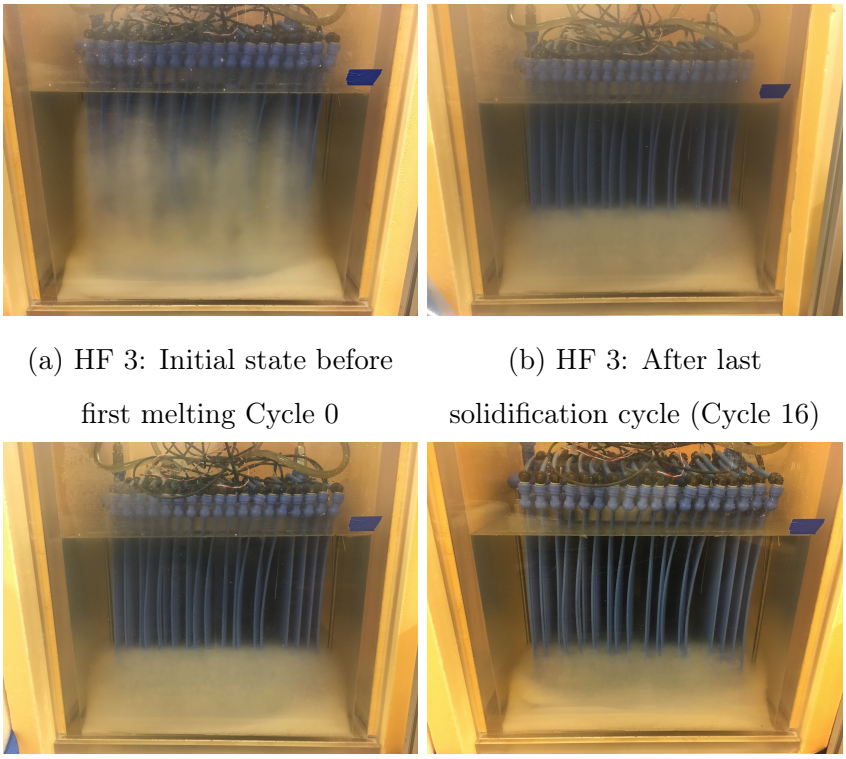

(a) HF 3: Initial state before first melting Cycle 0

(b) HF 3: After last solidification cycle (Cycle 16)

(c) HF 3: After last melting cycle (Cycle 16)

(d) LF 2: After last melting cycle (Cycle 9)

Figure 6: Photos of PCM TES for HF 3 and LF 2 (Insulation was only removed to take photos before and after each experiment).

(solidification) capacities of all six experiments. The measured discharged capacity for Cycle 0 is lower than the theoretical storage capacity of the complete tank $Q_{max}$ due to only the PCM layer surrounding the HEX being able to solidify in the tank (Fig. 6a).

Fig. 8 summarizes the measured charging and discharging capacity of continued cycling with reference to the measured discharged capacity of Cycle 0. From Fig. 8a it can be seen that only a fraction of 80-60 % of this storage

capacity can be charged again in Cycle 1. It follows then that the second measured discharge capacity (Cycle 1) is reduced considerably compared to Cycle 0 (Fig. 8b).

HF 1, HF 2 and LF 1 were the initial experiments performed on the tank. The experiments were stopped after initial observations of the reduced capacity in the tank. It was then decided to increase the number of cycles in experiments HF 3, MF 3 and LF 2 to study whether the capacity drop will stabilize with higher cycles.

It is notable that while the charging capacity maintains a higher value than the discharge capacity, both continue to drop significantly in subsequent cycles before stabilizing at a constant low value at higher cycles. This strongly indicates that the material behavior is especially unstable in the first melting cycles. The fact that the charging capacity decreases as well indicates that the PCM TES solidifies less with subsequent cycling for the given duration and temperature range. This is observable for all experiments and the capacity loss decreases more severely with lower mass flow rate settings. After 9 to 16 cycles only 60 % of the initial measured storage capacity can be repeatedly charged again within 12 hours, while 50-40 % can be discharged. Once the charging and discharging capacity stabilizes, the constant difference between charging and discharging capacity can be contributed to the energy losses of the PCM TES in a complete cycle, such as thermal losses to the ambient. They range from 0.5 to 0.26 kWh for LF 2 and HF 3 respectively (Fig. 7).

Fig. 9 shows the effective discharge capacities under cutoff conditions. It is remarkable that the capacity effectiveness drops considerably more for the

low mass flow rate case. Since the cutoff condition is reached earlier, the remaining latent heat can not be effectively utilized for the chosen temperature range and duration.

When comparing the effective storage densities in Fig. 9d, the storage is able to discharge between 50-40 % of its theoretical maximum capacity in the initial melting cycle. One reason for this deviation is the large amount of inactive PCM between the storage container wall and the heat exchanger tubes in the current setup. If can be expected that this deviation can be decreased if the physical gap between container wall and heat exchanger is decreased. However, due to the low discharge capacities with subsequent cycles, the effective storage density drops considerably in all experiments.

Cases LF 1 and HF 1 in Fig. 8a show a noticeably higher charging capacity compared to the other cases. From Fig. 10 it can be seen that the increased charging capacity for Cycle 1 of LF 1 compared to LF 2 is due to the top part of the PCM solidifying in LF 1 but not in LF 2. This can be concluded from the 10 cm sensors recorded a temperature increase from a supercooled state in LF 1. Additionally, due to the larger temperature difference in LF 1, the bottom part is able to finish solidification within 12 hours compared to LF 2. However, despite the high charging capacity for LF 1 and HF 1, the discharging capacity drops considerably from Cycle 1 to 3 similar to the other experiments. This indicates that the PCM TES is generally subject to a phenomenon decreasing the discharge capacity independent from the charged capacity of the first cycle.

Also, note the sensors T10-3 and T30-4 in Fig. 10, which follow the rest of the temperature sensors more slowly. Due to their near constant slope,

these sensors may appear to indicate a slow phase transition. However, it is more likely that these two sensors are in a position where the heat exchanger is not active. Therefore, readings from temperature sensors alone may not be enough to indicate phase transition taking place in the storage.

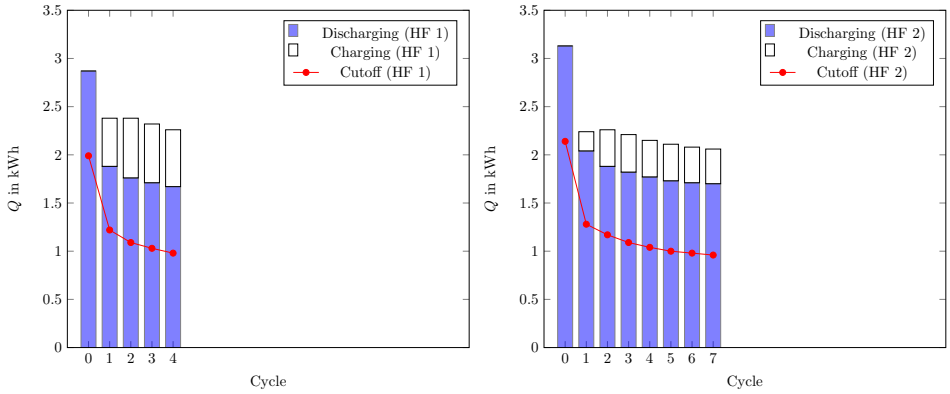


(a) HF 1




(b) HF 2

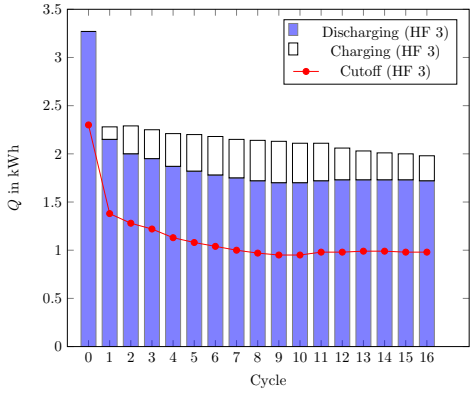


(c) HF 3

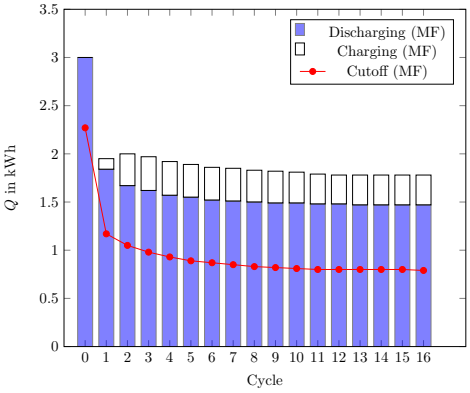


(d) MF

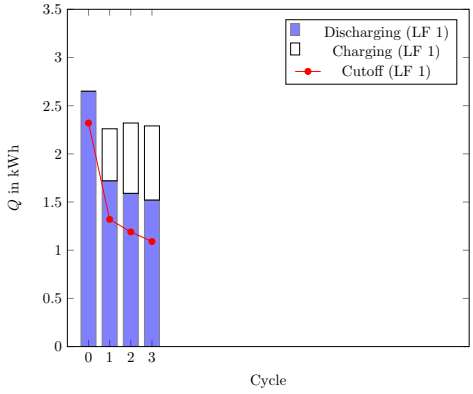


(e) LF 1

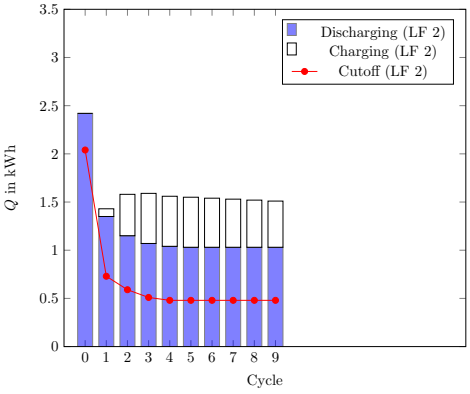


(f) LF 2

Figure 7: Measured discharging and charging capacities over subsequent cycling for all experiments

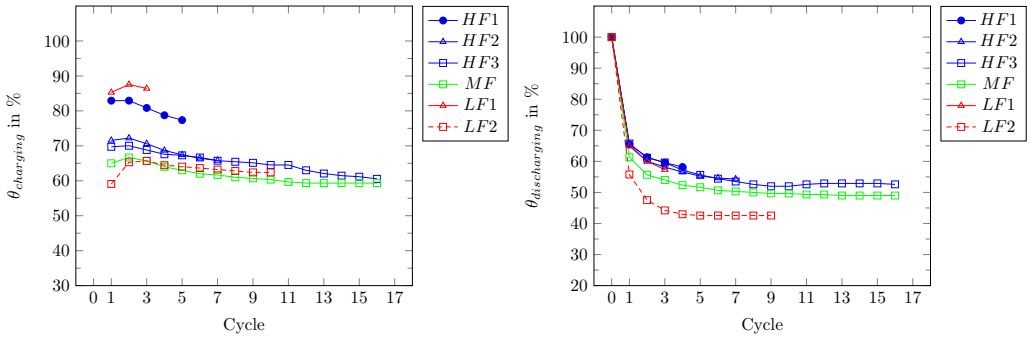


(a) Charging (Solidification):

$$\theta_{charging} = \frac{Q_{charging}}{Q_{discharging}(Cycle\ 0)}$$

(b) Discharging (Melting):

$$\theta_{discharging} = \frac{Q_{discharging}}{Q_{discharging}(Cycle\ 0)}$$

Figure 8: Measured discharging and charging capacities over subsequent cycling

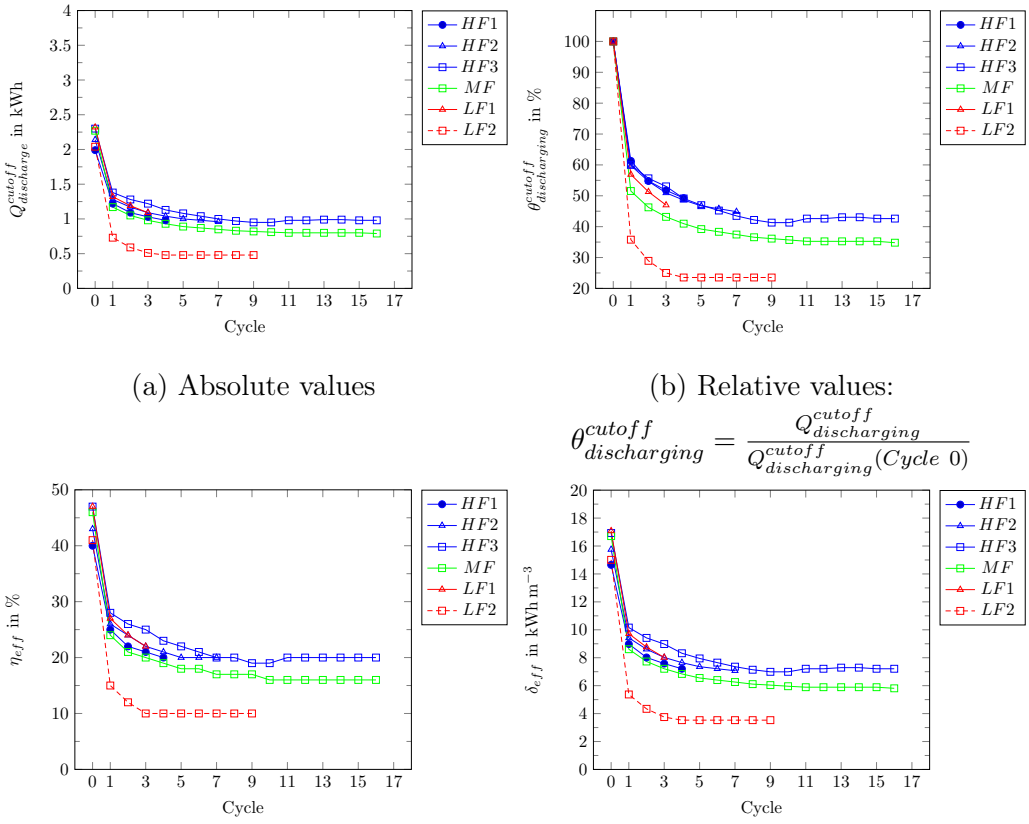


(a) Absolute values

(b) Relative values:

$$\theta^{cutoff}_{discharging} = \frac{Q^{cutoff}_{discharging}}{Q^{cutoff}_{discharging}(Cycle\ 0)}$$

(c) Capacity effectiveness

(d) Effective storage density

Figure 9: Measured discharge parameters under cutoff condition ($T_{out}(t = t^*) = 14\,°\mathrm{C}$) over subsequent cycling.

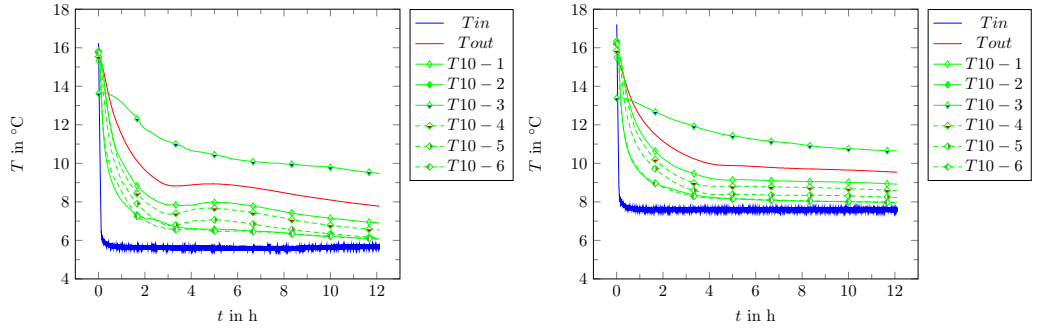


(a) LF 1




(b) LF 2

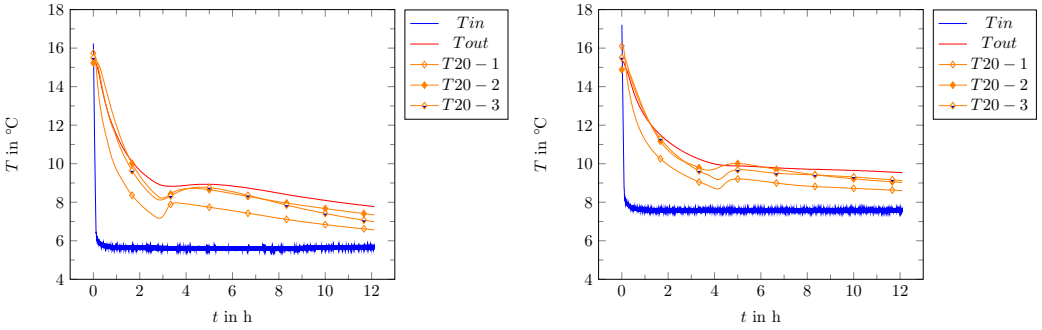


(c) LF 1




(d) LF 2

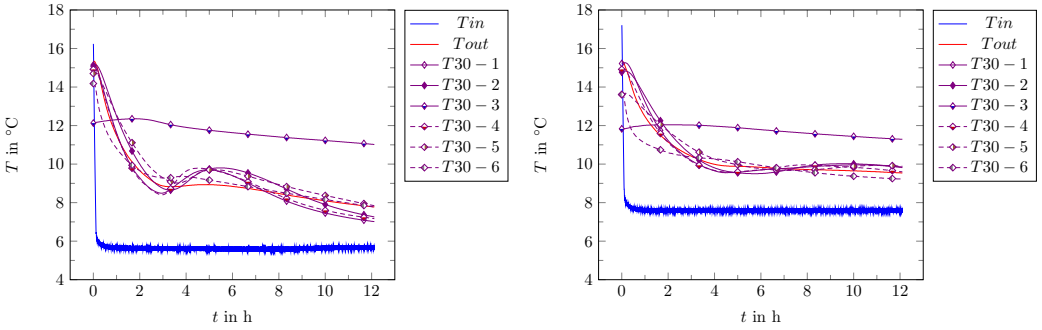


(e) LF 1




(f) LF 2

Figure 10: LF 1 & 2: Comparison of PCM temperature for the first solidification cycle. T10, T20 and T30 refer to individual temperature sensors at 10, 20 and 30 cm depth in the PCM TES, respectively.

Fig. 11 shows the measured in- and outlet temperatures for the first and last melting and solidification cycles of the experiments HF 3 (Cycle 0 to 16) and LF 2 (Cycle 0 to 9). For melting, the loss in latent storage capacity can be seen by the cutoff condition taking place considerably earlier. In all cases, the outlet temperatures indicate a transition from a latent heat storage to a storage storing only sensible heat right after the first melting cycle.

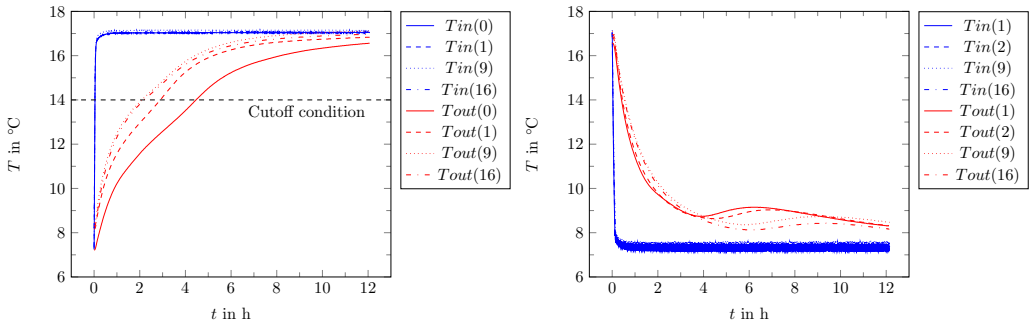


(a) HF 3: Melting




(b) HF 3: Solidification

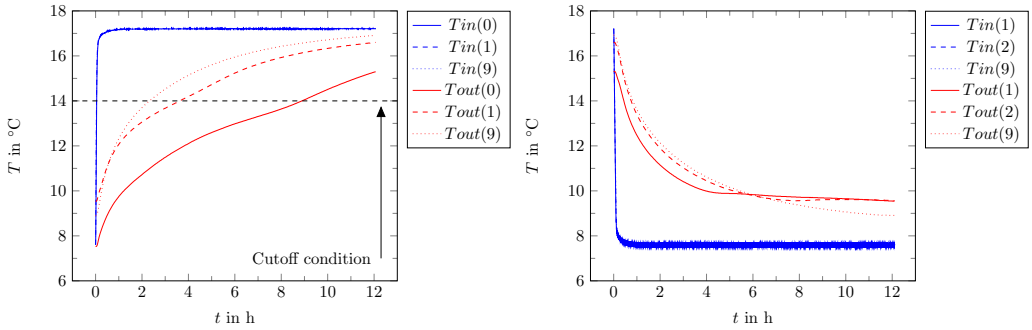


(c) LF 2: Melting




(d) LF 2: Solidification

Figure 11: Comparison of measured outlet temperatures with increasing melting and solidification cycles for the cases HF 3 and LF 2. The number in the brackets indicates the current cycle.

This is also confirmed in Fig. 12 to 15, which compare the exact PCM temperatures for the cases HF 3 and LF 2 for the first and ninth cycle.

For HF 3 in Fig. 12 and 13, it can be seen that the top and middle sensors indicate only sensible heat in Cycle 9 compared to Cycle 0 and 1. For the latter all top, middle and bottom sensors show phase transitions. However, in Cycle 9 only the bottom part shows obvious phase transitions for both melting and solidification. Moreover, the solidification from the supercooled state at the bottom part occurs delayed from Cycle 1 and 12 hours are not enough to complete the solidification (Fig. 13e and 13f). It can be concluded that with increasing cycling, the supercooling temperature of the PCM drops and top and middle section seem not to be actively solidifying compared to the bottom part. These temperatures are coherent with the photos of Fig. 6 which show no visible difference between the last melting and solidification cycle.

With a lower flow rate in case LF 2 (Fig. 14), also the bottom temperature sensors show only sensible heat storage in the ninth cycle. This explains the considerably lower storage capacities for discharging compared to HF 3. For the first solidification cycle of LF 2 (Fig. 15), the middle and bottom part shows supercooling down to 9 °C, while in the HF 3 case (Fig. 13) these parts supercool to a slightly lower temperature down to 8.5 °C.

It is possible that the solid phase, which is continuously present at the bottom part of the storage (see Fig. 6) does not necessarily provide a nucleation point of the surrounding supercooled liquid phase since an increase of supercooling is observed for the ninth cycle compared to the first cycle for both LF2 and HF3. From these observations it can be concluded that the

PCM has changed its composition as soon as after the first melting in Cycle 0. This change has caused a significant decrease of storage capacity of the PCM TES using the studied temperature ranges and cycling duration since major parts of the PCM TES are not actively storing latent heat.

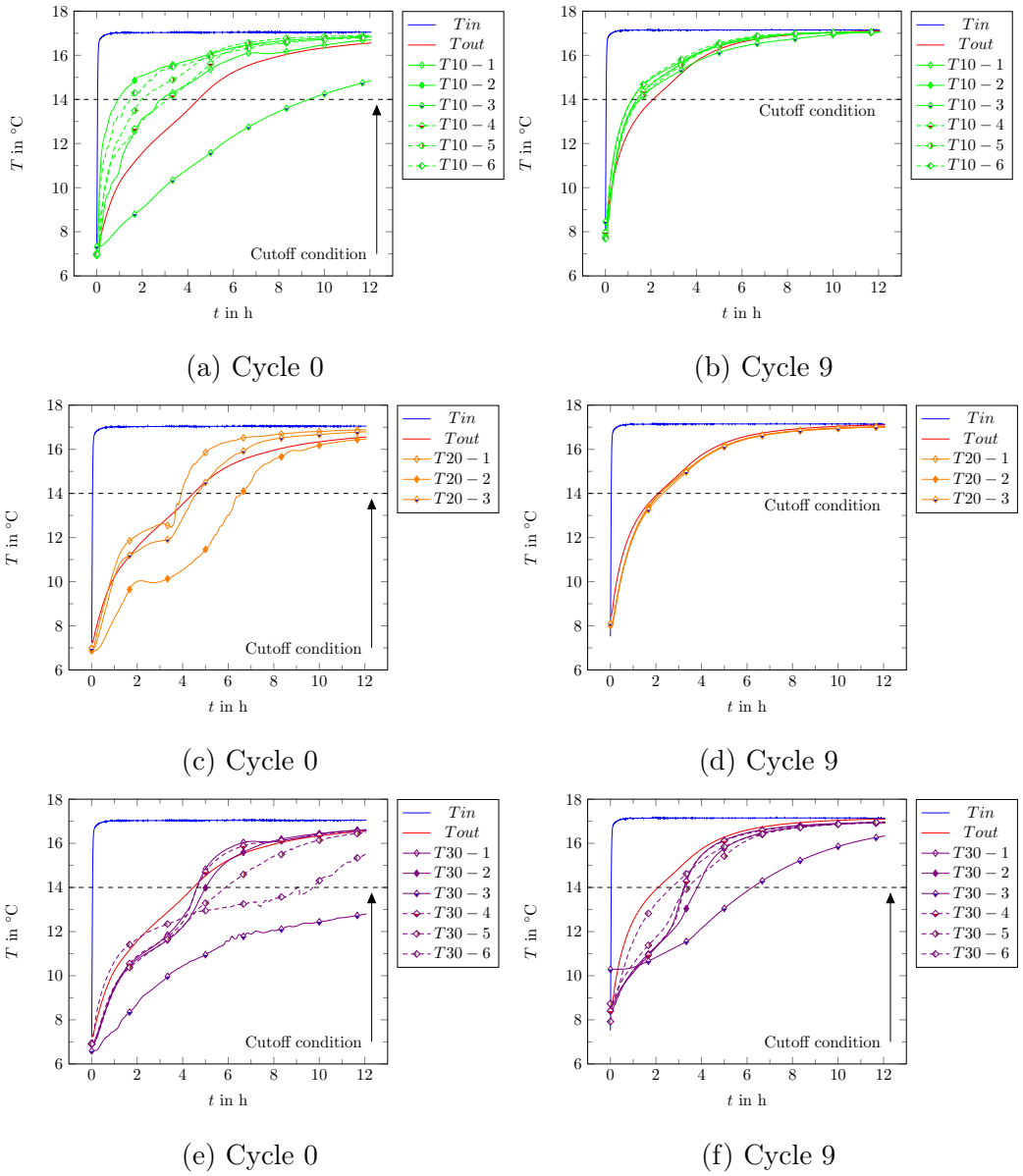


(a) Cycle 0

(b) Cycle 9

(c) Cycle 0

(d) Cycle 9

(e) Cycle 0

(f) Cycle 9

Figure 12: HF 3: Comparison of PCM temperature for melting Cycle 0 and 9. T10, T20 and T30 refer to individual temperature sensors at 10, 20 and 30 cm depth in the PCM TES, respectively.

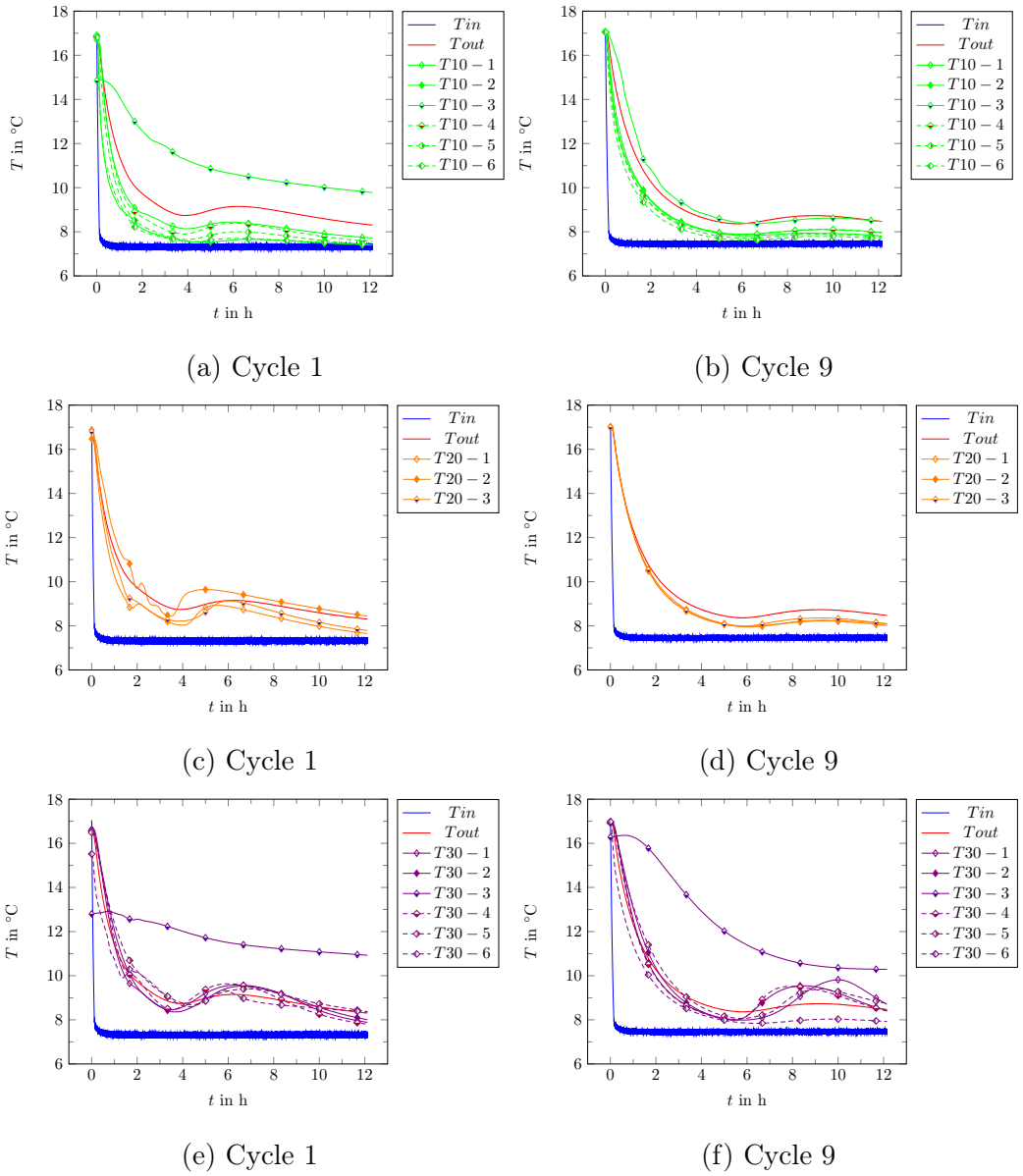


(a) Cycle 1

(b) Cycle 9

(c) Cycle 1

(d) Cycle 9

(e) Cycle 1

(f) Cycle 9

Figure 13: HF 3: Comparison of PCM temperature for solidification Cycle 1 and 9. T10, T20 and T30 refer to individual temperature sensors at 10, 20 and 30 cm depth in the PCM TES, respectively.

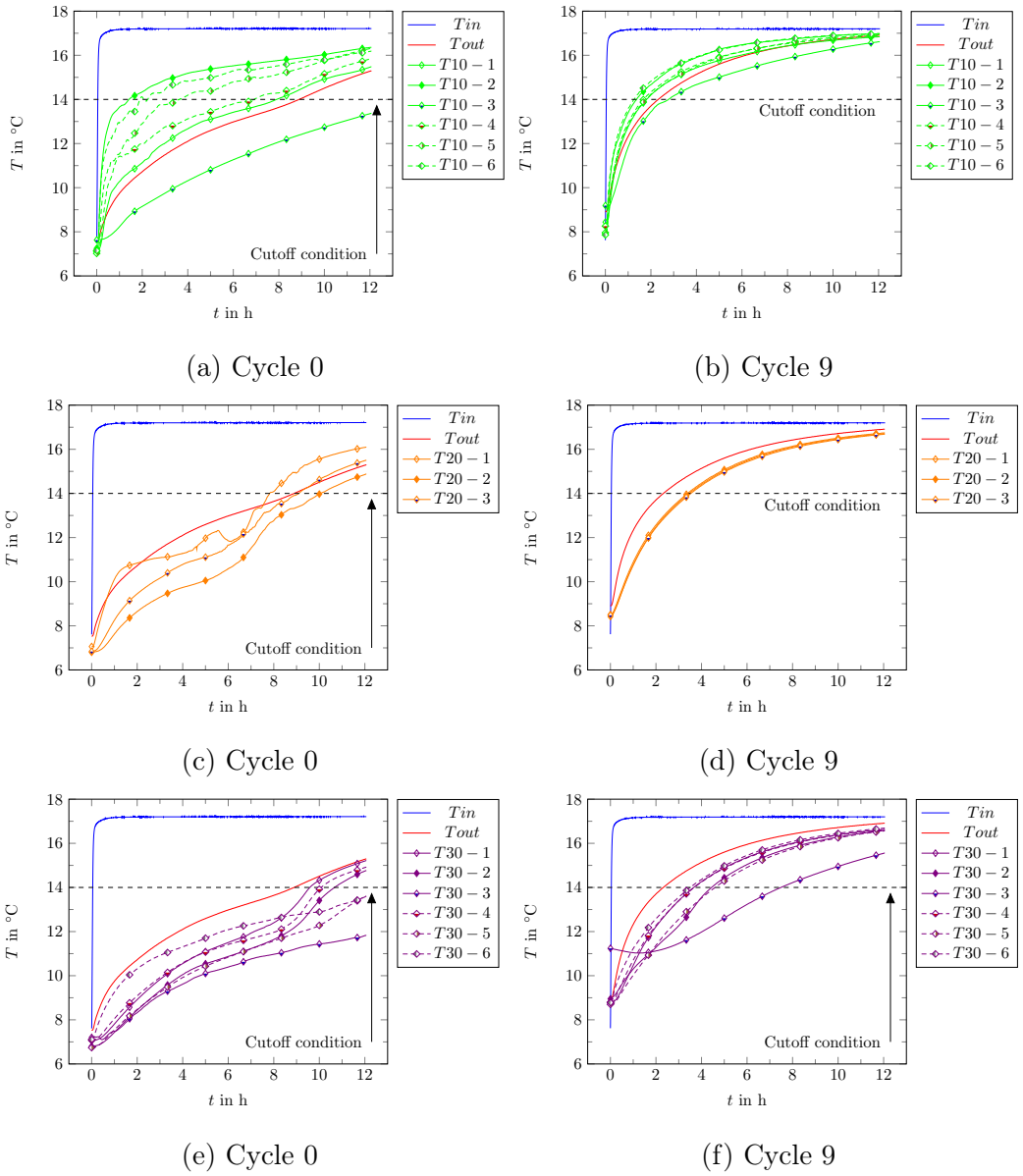


(a) Cycle 0

(b) Cycle 9

(c) Cycle 0

(d) Cycle 9

(e) Cycle 0

(f) Cycle 9

Figure 14: LF 2: Comparison of PCM temperature for melting Cycle 0 and 9. T10, T20 and T30 refer to individual temperature sensors at 10, 20 and 30 cm depth in the PCM TES, respectively.

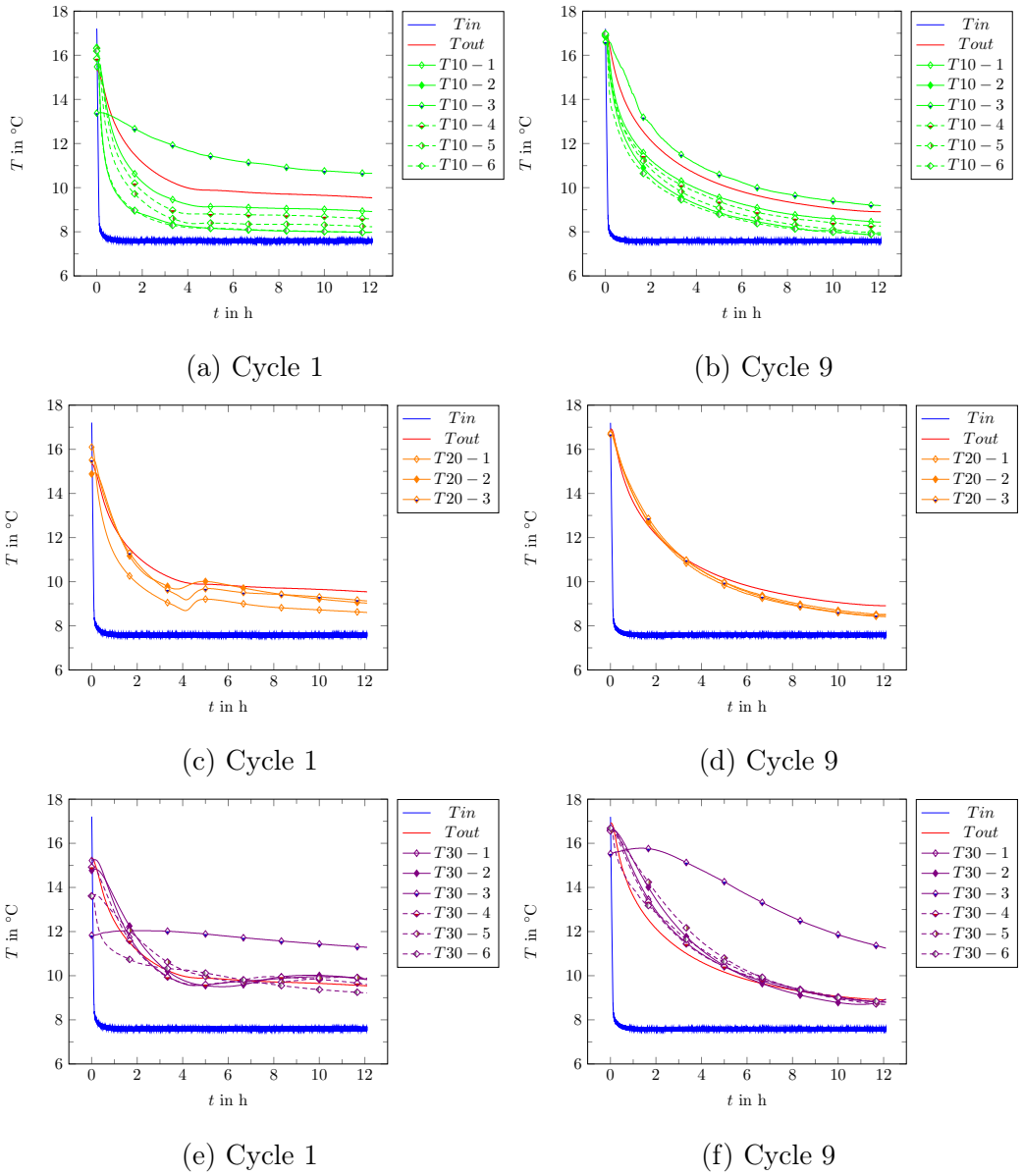


(a) Cycle 1

(b) Cycle 9

(c) Cycle 1

(d) Cycle 9

(e) Cycle 1

(f) Cycle 9

Figure 15: LF 2: Comparison of PCM temperature for solidification Cycle 1 and 9. T10, T20 and T30 refer to individual temperature sensors at 10, 20 and 30 cm depth in the PCM TES, respectively.

*3.4. Sample Analysis using T-History method*

T-History measurements according to a previously validated experimental setup described in [26] were performed from samples of the storage PCM to understand the mechanisms behind the storage capacity degradation. Four 15 mg samples were taken at 1/3 (13 cm) and 2/3 (27 cm) height of the PCM TES before and after cycling HF 3 (Fig. 1b). The samples were cycled in a climate chamber by changing the ambient temperature in the chamber between 20 °C and 1 °C.

Fig. 16 shows the measured enthalpy curves from the two different storage heights before cycling the PCM TES. It can be seen that even at the initial state, the liquid PCM show a different composition depending on the location. The side B top sample at 1/3 height shows increased supercooling down to <4 °C as well as a shift to lower melting temperature of 2 °C compared to the side B bottom sample. The same trend is observable with the Side A sample. This finding explains why the top part of the storage is not able to solidify with a charging temperature of 8 °C. All bottom samples taken before cycling on the other hand show stable solidification and melting with a supercooling degree of 10.5 °C and a melting range between 12-14 °C. The measured storage capacity (8-18 °C) of the bottom and top samples is within 0.0325-0.222 $\mathrm{kW\,h\,kg^{-1}}$, respectively. This is in the range of the reported 0.0293 $\mathrm{kW\,h\,kg^{-1}}$ from the manufacturer.

For the samples taken from the PCM TES after cycling, Side A and B yielded different results. For Side A, it can be seen that the bottom composition has changed significantly to lower storage capacity, supercooling temperature and melting temperature compared to the Side A samples before

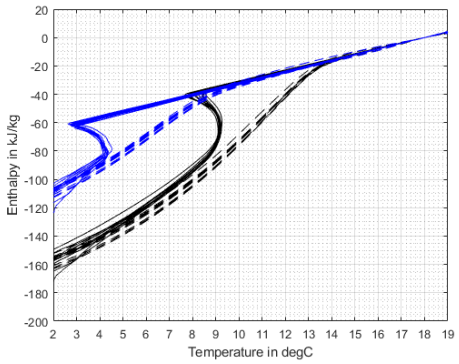


(a) Side A - Top Sample (from 1/3 height)

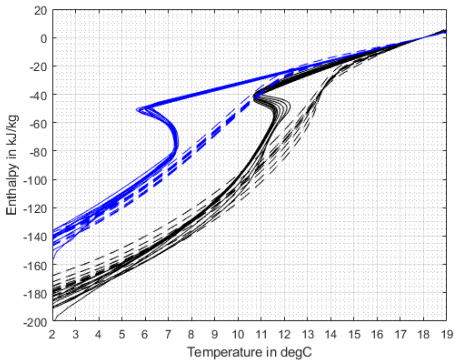


(b) Side A - Bottom Sample (from 2/3 height)

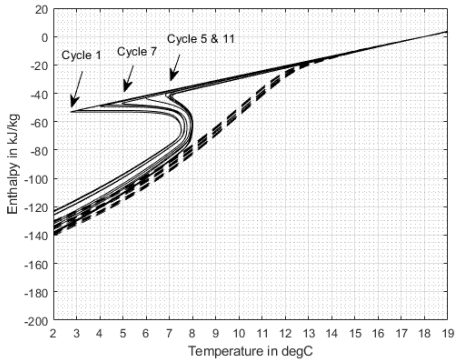


(c) Side B - Top Sample (from 1/3 height)

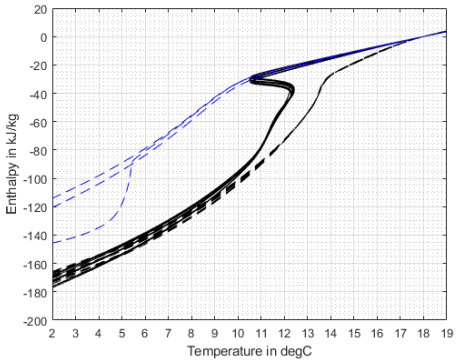


(d) Side B - Bottom Sample (from 2/3 height)

Figure 16: Enthalpy versus temperature curves of samples taken from the tank before (color: black) and after (color: blue) cycling. The samples are taken from different locations of the tank according to Fig. 1b. Each sample was measured using 11 melting (dashed line) and solidification (solid line) cycles. Normalization of enthalpy values at 18 °C. In (c) the different degrees of supercooling per cycle appears to be random and not systematic.

cycling. For Side B, only three solidification and melting occasions were recorded for the bottom sample (see Fig. 16d). The sample supercooled down to 1.2 °C. Here also a shift to lower melting temperature is observable. In all other occasions it did not solidify at all. For the side B top sample taken after cycling the PCM TES, no solidification and melting was recorded. Here the sample likely supercools and/or melts outside of the experimental range.

Since the samples do not show a degradation after continued T-History cycles, incongruent melting of the liquid PCM is unlikely the main reason for the observed rapid storage capacity decrease. Instead, it is more likely caused by different liquid phases with different densities being present across the height of the PCM storage. The top liquid phases are of lower density and are not suitable for storing latent heat in the application temperature range due to increased degree of supercooling and lower solidification temperature. The results from the samples taken after cycling the PCM TES indicate that the liquid phases have separated further with consecutive cycling of the storage. After 16 cycles, the phases distributed across at least 2/3 of the heat exchanger height are not suitable for storing latent heat in the application temperature range.

Figure 17 provides an overview of the observations in this work.

### *3.5. Summary of Discussion*

The T-History sample measurements show that it is likely that the PCM TES design and operation mode facilitate a separation of different liquid phases across the storage height. This then leads to phases that do not melt and solidify in the declared operative temperature range, due to supercooling

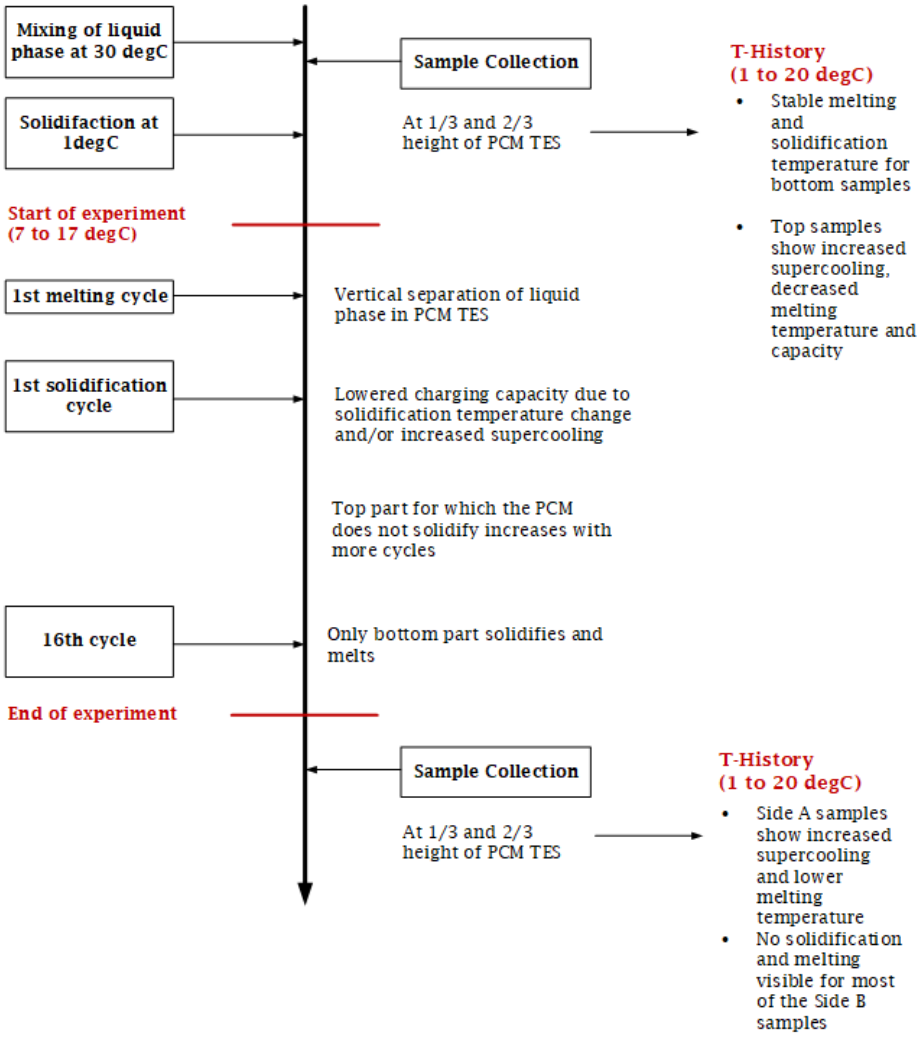


Figure 17: Overview of conclusions for experiment HF 3

and/or a shift of melting and solidification temperature. Incongruent melting was not observed from the samples before cycling the PCM TES, but it can not be excluded that the separated liquid phase compositions experience this problem. It was not possible to check whether the samples taken after cycling the storage experience incongruent melting, since these samples did not solidify and melt in the T-History experiments.

Since the capacity loss is already observed after the first melting cycle, it is likely that this phase separation happens more pronounced during melting compared to solidification. The liquid phase always present in the tank, due to the large gap between storage container and heat exchanger, also likely enhances this separation.

## 4. Conclusions

A commercial PCM TES design using a commercial salt-hydrate as storage material has been experimentally evaluated for a cold storage application in a laboratory unit. It was observed that the measured charging and discharging capacity decreased severely after only a few cycles due to phase separation. The PCM TES under phase separation has a lower effective storage density than water for the given temperature range.

Moreover, a notable observation was that the laboratory storage performs considerably worse compared to T-History experiments in terms of phase separation and supercooling. For the former, it can be explained that the liquid PCM contains multiple phases of different densities that can distribute along the height of the storage. In case of T-History experiments, the sample is constrained into a small volume, which suppresses immediate liquid phase

separation. A higher degree of supercooling is measured in the PCM TES compared to in the T-History experiments. This is a different observation from previous studies [10], where the larger size and existence of A solid phase inside the tank would suppress this phenomenon. Due to phase separation of the liquid phase in this study, the solid phase in this storage does not necessarily contribute to nucleation of a supercooled liquid. Therefore, an analysis of the composition of the solid and liquid phases, before and after phase separation, would be therefore necessary to explain these observations.

For the studied PCM TES design, several aspects need to be considered in future work:

1. The current storage design does not guarantee a stable performance using SP11 since phase separation can occur as early as after the first melting cycle. Since the liquid phases separate, it is likely enhanced if the design allows a convective liquid phase.
2. Operation of the storage appears to have an effect on the severeness of phase separation, especially at lower mass flow rates for charging and discharging. At higher mass flow rates it appears that a higher rate of solidification/melting leads to a lower rate of phase separation.
3. When the storage capacity decreases, it is recommended to charge the storage at higher flow rates in order to solidify more PCM within the same charging duration.
4. Storage density in this design can be generally increased by reducing the volume of inactive PCM between the heat exchanger and container wall. This also constrains a convective liquid phase in order to decrease the potential for phase separation.

5. Moreover, the current geometry of the capillary tubes in the heat exchanger should be investigated in terms of its optimum capacity effectiveness for the chosen cutoff condition. The work of Fang et al. [27, 28] showed that there exists an optimum configuration depending on the effective thermal conductivity of the PCM.

An important takeaway is that measurements on smaller samples can only verify that the investigated PCM composition does not degrade due to incongruent melting. This may explain why the manufacturer of the PCM initially did not consider phase separation to be a problem with the heat exchanger design. Since it is shown here that the separation of liquid phases is possible in commercial mixtures, which degrades the storage capacity immediately after the first cycle. Therefore observations on a larger scale are necessary to make this phenomenon observable.

On a positive note, it has also been shown that the phase separation in the storage can be relatively simply reversed by following the procedure outlined in section 3.1, when both a large range of process temperatures is available and mixing of the PCM is possible.

**Acknowledgments**

This work was carried out as part of the first author's PhD studies. The funding provided by the Swedish Energy Agency (Energimyndigheten) within the E2B2 program (grant no. 39695-1) and from the Swedish Environmental Protection Agency (grant no. NV-07079-16) is gratefully acknowledged.

## References


[1] P. Tatsidjodoung, N. Le Pierrès, L. Luo, A review of potential materials for thermal energy storage in building applications, Renewable and Sustainable Energy Reviews 18 (2013) 327–349. doi:10.1016/j.rser.2012.10.025.

[2] B. Zalba, J. M. Marín, L. F. Cabeza, H. Mehling, Review on thermal energy storage with phase change: materials, heat transfer analysis and applications, Applied Thermal Engineering 23 (3) (2003) 251–283. doi:10.1016/S1359-4311(02)00192-8.

[3] H. Mehling, L. F. Cabeza, Heat and cold storage with PCM: An up to date introduction into basics and applications; with 28 tables, Heat and Mass Transfer, Springer, 2008.

[4] M. Aneke, M. Wang, Energy storage technologies and real life applications – a state of the art review, Applied Energy 179 (2016) 350–377. doi:10.1016/j.apenergy.2016.06.097.

[5] M. Kenisarin, K. Mahkamov, Salt hydrates as latent heat storage materials: Thermophysical properties and costs, Solar Energy Materials and Solar Cells 145 (2016) 255–286. doi:10.1016/j.solmat.2015.10.029.

[6] S. A. Mohamed, F. A. Al-Sulaiman, N. I. Ibrahim, M. H. Zahir, A. Al-Ahmed, R. Saidur, B. S. Yılbaş, A. Z. Sahin, A review on current status and challenges of inorganic phase change materials for thermal energy storage systems, Renewable and Sustainable Energy Reviews 70 (2017) 1072–1089. doi:10.1016/j.rser.2016.12.012.

[7] E. Oró, L. Miró, C. Barreneche, I. Martorell, M. M. Farid, L. F. Cabeza, Corrosion of metal and polymer containers for use in pcm cold storage, Applied Energy 109 (2013) 449–453. doi:10.1016/j.apenergy.2012.10.049.

[8] S. Ushak, P. Marín, Y. Galazutdinova, L. F. Cabeza, M. M. Farid, M. Grágeda, Compatibility of materials for macroencapsulation of inorganic phase change materials: Experimental corrosion study, Applied Thermal Engineering 107 (2016) 410–419. doi:10.1016/j.applthermaleng.2016.06.171.

[9] A. Safari, R. Saidur, F. A. Sulaiman, Y. Xu, J. Dong, A review on supercooling of phase change materials in thermal energy storage systems, Renewable and Sustainable Energy Reviews 70 (2017) 905–919. doi:10.1016/j.rser.2016.11.272.

[10] C. Rathgeber, H. Schmit, L. Miró, Cabeza L. F., A. Gutierrez, S. Ushak, S. Hiebler, A. Hauer, Analysis of supercooling of phase change materials with increased sample size - comparison of measurements via dsc, t-history and at pilot plant scale, in: Proceedings in Greenstock 2015 - 13th IEA ECES Conference, 2015.

[11] C. Rathgeber, H. Schmit, L. Miró, L. F. Cabeza, A. Gutierrez, S. N. Ushak, S. Hiebler, Enthalpy-temperature plots to compare calorimetric measurements of phase change materials at different sample scales, Journal of Energy Storage 15 (2018) 32–38. doi:10.1016/j.est.2017.11.002.

[12] G. A. Lane, Solar Heat Storage: Latent Heat Materials, Vol. I: Background and Scientific Principles, CRC Press, 1983. doi:10.1115/1.3266412.

[13] G. A. Lane, Solar Heat Storage: Latent Heat Materials, Vol.II: Technology, CRC Press, 1986.

[14] M. K. Rathod, J. Banerjee, Thermal stability of phase change materials used in latent heat energy storage systems: A review, Renewable and Sustainable Energy Reviews 18 (2013) 246–258. doi:10.1016/j.rser.2012.10.022.

[15] W. Kong, M. Dannemand, J. Brinkø Berg, J. Fan, G. Englmair, J. Dragsted, S. Furbo, Experimental investigations on phase separation for different heights of sodium acetate water mixtures under different conditions, Applied Thermal Engineering 148 (2019) 796–805. doi:10.1016/j.applthermaleng.2018.10.017.

[16] S. N. Gunasekara, S. Kumova, J. N. Chiu, V. Martin, Experimental phase diagram of the dodecane-tridecane system as phase change material in cold storage, International Journal of Refrigeration- doi:10.1016/j.ijrefrig.2017.06.003.

[17] H. A. Zondag, R. de Boer, S. F. Smeding, J. van der Kamp, Performance analysis of industrial pcm heat storage lab prototype, Journal of Energy Storage 18 (2018) 402–413. doi:10.1016/j.est.2018.05.007.

[18] M. Alam, P. X. Zou, J. Sanjayan, S. Ramakrishnan, Energy saving performance assessment and lessons learned from the oper-

ation of an active phase change materials system in a multi-storey building in melbourne, Applied Energy 238 (2019) 1582–1595. doi:10.1016/j.apenergy.2019.01.116.

[19] M. Jokiel, Development and performance analysis of an object-oriented model for phase change material thermal storage: Project report, sintef (2016).

[20] IEA ECES Annex 30, Applications of thermal energy storage in the energy transition - benchmarks and developments: Public report (september 2018).

[21] P. Tan, M. Brütting, S. Vidi, H.-P. Ebert, P. Johansson, A. Sasic Kalagasidis, Characterizing phase change materials using the t-history method: On the factors influencing the accuracy and precision of the enthalpy-temperature curve, Thermochimica Acta 666 (2018) 212–228. doi:10.1016/j.tca.2018.07.004.

[22] Rubitherm GmbH, https://www.rubitherm.eu/.

[23] BEKA Heiz- und Kühlmatten GmbH, https://www.beka-klima.de/en/ice-energy-storage/.

[24] Joint Committee for Guides in Metrology, Evaluation of measurement data - supplement 1 to the "guide to the expression of uncertainty in measurement": Propagation of distributions using a monte carlo method (jcgm 101:2008).

[25] M. Solaguren-Beascoa Fernández, J. M. Alegre Calderón, P. M. Bravo Díez, Implementation in matlab of the adaptive monte carlo method for

the evaluation of measurement uncertainties, Accreditation and Quality Assurance 14 (2) (2009) 95–106. doi:10.1007/s00769-008-0475-6.

[26] P. Tan, On the design considerations for thermal energy storage with phase change materials: Material characterization and modelling, Licentiate thesis, Chalmers University of Technology (2018).
URL https://research.chalmers.se/publication/500367

[27] Y. Fang, J. Niu, S. Deng, Numerical analysis for maximizing effective energy storage capacity of thermal energy storage systems by enhancing heat transfer in pcm, Energy and Buildings 160 (2018) 10–18. doi:10.1016/j.enbuild.2017.12.006.

[28] Y. Fang, J. Niu, S. Deng, An analytical technique for the optimal designs of tube-in-tank thermal energy storage systems using pcm, International Journal of Heat and Mass Transfer 128 (2019) 849–859. doi:10.1016/j.ijheatmasstransfer.2018.08.138.